Journal of Computational Neuroscience 8, 51–63 (2000)

On the Simulation of Large Populations of Neurons

A. OMURTAG
Laboratory of Applied Mathematics, Mount Sinai School of Medicine, One Gustave L. Levy Place, New York, NY 10029
ahmet@camelot.mssm.edu

B.W. KNIGHT
The Rockefeller University, 1230 York Avenue, New York, NY 10021; Laboratory of Applied Mathematics, Mount Sinai School of Medicine, One Gustave L. Levy Place, New York, NY 10029

L. SIROVICH
Laboratory of Applied Mathematics, Mount Sinai School of Medicine, One Gustave L. Levy Place, New York, NY 10029; The Rockefeller University, 1230 York Avenue, New York, NY 10021

Received December 29, 1998; Revised March 12, 1999; Accepted April 21, 1999

Action Editor: John Rinzel

Abstract. The dynamics of large populations of interacting neurons is investigated. Redundancy present in subpopulations of cortical networks is exploited through the introduction of a probabilistic description. A derivation of the kinetic equations for such subpopulations, under general transmembrane dynamics, is presented.

The particular case of integrate-and-fire membrane dynamics is considered in detail. A variety of direct simulations of neuronal populations, under varying conditions and with as many as $O(10^5)$ neurons, is reported. Comparison is made with analogous kinetic equations under the same conditions. Excellent agreement, down to fine detail, is obtained. It is emphasized that no free parameters enter in the comparisons that are made.

Keywords:

1. Introduction

The ability to faithfully simulate interacting neural populations can significantly deepen our understanding of neural network function. However, even very elementary estimates show this to be a very daunting goal. Our initial challenge, the mammalian primary visual cortex, has $O(10^8)$ neurons, many of which make contact with $O(10^4)$ other neurons. The underlying dynamics of individual neurons, which contain a variety of voltage dependent ionic channels, requires complex Hodgkin-Huxley-like systems of differential equations. The time scales of the dynamics range from fractions of a millisecond to at least many seconds. In spite of these obstacles some limited but important attempts at simulation have appeared (Worgotter and Koch, 1991; Chee-Orts et al., 1996), and recently Somers et al. (1995) have generated a serious simulation of an orientation hypercolumn of the visual cortex. This last simulation has been very valuable in many ways; most particularly, it has considerably sharpened the lines in the controversy that surrounds the nature and origin of orientation tuning in the visual cortex (Hubel and Wiesel, 1962;

Albrecht and Geisler, 1994; Sillito, 1975; Ferster et al., 1996).

The simulations mentioned above are of the type called direct simulations, which are discussed below in Section 3. In brief this is an approach based on following the dynamics of individual neurons that are connected to other neurons according to a specified wiring blueprint and synaptic dynamics.

In this article we present another approach, which seeks to make use of the redundancy that appears in the cortex. To some degree our approach is motivated by the highly suggestive results that are now emerging from optical imaging (Blasdel, 1992a, 1992b; Grinvald et al., 1991; Sirovich et al., 1996). These and other results imply that the cortex is tiled by patches of tissue that correspond to the visual modalities. Nominally, the *patches* that are involved in like activity are found to contain $O(10^4)$ neurons. On this basis we approach the task of simulating an ensemble of interacting neurons by means of a statistical description of the population. Historically, our approach is newer and less studied than direct simulation. An early effort, along essentially modern lines, appears in the thesis of Johannesma (1969). Our approach is based on an early effort by one of us (Knight, 1972) and the more recent expositions (Knight et al., 1996; Knight, 1998; see also Sirovich et al., 1998, where this approach is used to obtain equilibrium solutions, and Nykamp and Tranchina, 1998). Other allied treatments have been presented by Kuramoto (1991) and Abbott and van Vreeswijk (1991). In this connection we also mention the related *mean field approximations* found in Sompolinsky et al. (1991), McLaughlin et al. (1998), and Chawanya et al. (1993).

2. Theoretical Principles

In what follows we develop two contrasting frameworks for describing the evolution of subpopulations of neurons. The term *subpopulation* here refers to an essentially homogeneous collection of interacting neurons or *encoders*, the internal states of which vary in time. In general the neurons of a subpopulation interact with one another and may couple to other subpopulations.

The internal state of a neuron is specified by a set of biophysical variables that includes its membrane potential and also several variables that specify the conductances of ionic channels. For the original Hodgkin-Huxley (H-H) system, which describes the electrophysiology of the giant squid axon, the state is specified by $\mathbf{v} = (v_1, v_2, v_3, v_4) = (V, m, h, n)$, where V is the membrane potential and where m governs sodium activation, h sodium inactivation, and n potassium activation. In this instance the neuronal state space is four dimensional. For complex neurons, such as LGN relay cells or electrically compartmentalized neurons (Keener and Sneyd, 1998; Segev et al., 1995), the dimension of state space can be quite large.

In the general case we regard the state of a neuron $\mathbf{v}$ to be governed by the dynamical system

$$\frac{d\mathbf{v}}{dt} = \mathbf{F}(\mathbf{v}) + \mathbf{S}(\mathbf{v}, g(t)). \tag{1}$$

For example, the direction field $\mathbf{F}$ could be that of the H-H-like system. $\mathbf{S}(\mathbf{v}, g(t))$ refers to the incoming synaptic *currents* to the neuron and as indicated generally depends on $\mathbf{v}$ as well as conductance $g(t)$. Generally, a number of conductances can be involved. For expository reasons only one is considered here.

The view we take is that synaptic arrivals cause conductance changes $g(t)$, which in turn produce the currents. As a matter of convention we regard the first equation of (1) as describing the membrane potential, $v_1 = V$. For example, in the context of the H-H system, in a standard notation (see Keener and Sneyd, 1998), the system (1) is

$$\left.\begin{aligned}
\frac{dV}{dt} &= \frac{1}{C}\{g_N m^3 h(V_N - V) + g_K n^4 (V_K - V) \\
&\qquad + g_L(V_L - V)\} + \frac{1}{C}\{g_s(t)(V_s - V)\}. \\
\frac{dm}{dt} &= \frac{1}{\tau_m(V)}(m_\infty(V) - m) \\
\frac{dh}{dt} &= \frac{1}{\tau_h(V)}(h_\infty(V) - h) \\
\frac{dn}{dt} &= \frac{1}{\tau_n(V)}(n_\infty(V) - n).
\end{aligned}\right\} \tag{2}$$

As indicated above, the variables (m, h, n) for H-H would be (v_2, v_3, v_4), so that the first bracketed term in the first equation is the first element of the vector $\mathbf{F}$—namely, $F_1(\mathbf{v})$. The last term of in this equation is the first component and only component of $\mathbf{S}$, $S_1(\mathbf{v}, g(t))$ and represents conductance changes due to synaptic arrivals. More generally, a range of excitatory and inhibitory conductances can appear so that for each of

these V_s refers to the appropriate reversal potential. For the H-H system S_1 is the only nonzero entry of **S**, but in more general situations, for example when calcium concentration plays a role, **S** may contain additional entries.

A heavily used illustrative case, below and in the literature, is the leaky (or forgetful) integrate and fire model of neuronal activity (Knight, 1972; Tuckwell, 1988; Peskin, 1975; Mirollo and Strogatz, 1990; Abbott and van Vreeswijk, 1993). In this case, the membrane potential V is governed by

$$C\frac{dV}{dt} = S(t) - \frac{1}{R}(V - V_r), \tag{3}$$

where C is the capacitance, R the resistance, and $S(t)$ the current associated with the neuron's membrane. When the membrane potential reaches threshold V_T, it is reset to the resting value V_r. If we set

$$v = \frac{V - V_r}{V_T - V_r}, \quad s = \frac{S}{C(V_T - V_r)}, \quad \gamma = \frac{1}{RC}, \tag{4}$$

then

$$\frac{dv}{dt} = -\gamma v + s(t), \quad 0 \le v \le 1. \tag{5}$$

Equation (5) is a minimal form of the integrate-and-fire model and will be used as a basis for later extension. This Eq. (5) is the single dynamical equation governing the single state variable v and in a sense represents the simplest form that the system (1) can assume.

The two frameworks we consider represent philosophically different approaches for describing the behavior of subpopulations. First, in the next section, we will describe direct simulations, in which the wiring of the network is specified and we follow the dynamics of each neuron. The second approach, presented in Section 4, follows the subpopulation via a *statistical mechanics*. In a well-defined sense, the population approach is exactly defined by the dynamical system of the direct approach. Finally, in the last section we compare the two approaches through numerical simulations.

3. Direct Simulation

Direct simulation furnishes us with the gold standard by which to compare any further modeling.

We enumerate the members of the assembly of neurons so that

$$\mathbf{v}^j = \mathbf{v}^j(t) \tag{6}$$

specifies the state of the jth neuron at time t. Each neuron of the homogeneous subpopulation follows a time course governed by

$$\frac{d}{dt}\mathbf{v}^j = \mathbf{F}(\mathbf{v}^j) + \mathbf{S}(\mathbf{v}^j, g^j(t)), \tag{7}$$

where the function **F**, the jth direction field, is the same for all neurons, but the conductance $g^j(t)$, varies with the neuron. The *current* to the jth neuron is due to synaptic arrivals from all neurons of the population as well as sources external to the population. Although we continue within the generality of (7), for purposes of exposition we make some inessential simplifying assumptions. Since typical synaptic time scales are relatively brief, we will ignore them. For the same reason we will ignore the delay in time that occurs in neuronal signaling.

Next we denote the firing times of the lth neuron by $\{t_n^l\}$, so this neuron connected to any other neuron will produce in it the conductance changes given by

$$g_l(t) = \hat{g}\sum_n \delta\left(t - t_n^l\right). \tag{8}$$

This states that a synaptic arrival will appear in the conductance as an impulse of fixed strength $\hat{g}$. Once the circuitry of the network is fixed, we can determine the set Γ^j of indices such that $l \epsilon \Gamma^j$ implies that the lth neuron is presynaptically connected to the jth neuron. Thus $g^j(t)$ is given by

$$g^j(t) = \sum_{l\epsilon\Gamma^j} g_l = \hat{g}\sum_{l\epsilon\Gamma^j}\sum_n \delta\left(t - t_n^l\right). \tag{9}$$

Provisionally, the circuitry is fixed by letting each neuron receive inputs from an average of G distinct randomly chosen other neurons (and hence sends out, on average, G afferents). (G, in effect, is the feedback gain.) The zero subscript sequence of times t_l denotes synaptic arrival times from external sources. In actual simulations this is drawn from a Poisson distribution, individually selected for each neuronal encoder.

The selection of a circuitry bears further discussion. As indicated above, neuronal connections are chosen at random so that on average each neuron has G afferents. The so chosen *blueprint* of interconnections may be

thought of as a matrix drawn from an ensemble of such connectivity matrices. There are several reasons why this matrix should be chosen anew at each neuronal firing. First, if this is not done, a particular choice of a matrix confers an identity on each neuron, and this is contrary to the hypothesis that all members of the population are on an equal footing. Second, laboratory observations show that synapses can have a significant failure rate (Abeles, 1991).

Finally, it is well known that assemblies of interconnected *oscillators* are capable of synchrony even under steady stimulation (Peskin, 1975; Mirollo and Strogatz, 1990; Golomb and Rinzel, 1993; Gerstner et al., 1996; Usher et al., 1993; Kuramoto, 1991; Abbott and van Vreeswijk, 1993; Tsodyks et al., 1993), and if the connectivity matrix is fixed physically, local oscillations can appear. However, in the limit of relatively sparse feedback we have verified computationally that simulations with a fixed matrix will produce the same results as those gotten from the temporally stochastic matrix. Synchronous versus asynchronous behavior is closely connected to the stability analysis of equilibrium solutions, the asynchronous state. This issue has been addressed analytically in the case of all-to-all coupling with synaptic failures. We have confirmed that the theoretical limit of feedback strength, which leads to instability of the asynchronous state, agrees with the common empirical limit that is observed for *both* simulations with synaptic failure and simulations with sparse interconnections. The loss of stability that occurs under feedback results in (at least) partial synchrony (Sirovich et al., 1999) and may be related to its occurrence in experiment (see Singer and Gray, 1995).

In principle, these remarks indicate how to fully specify the dynamical system (7), and the dynamics then follows from integration. It should be mentioned that in all the simulations reported here we are well away from the synchronous state.

For the purposes of exposition we have kept the development of this section simple. Several extensions will be given below in the illustrations—namely, stochastic $\hat{g}$, inhibitory connections, and interacting subpopulations.

4. Population Equations

There is an alternative to the direct computation of the detailed time-course of every neuron as demanded in a direct simulation. Instead, we can turn to a probabilistic description of the manner in which the whole population is distributed, in analogy with the view adopted in statistical mechanics. In more detail we envision following the evolution of a probability density $\rho = \rho(\mathbf{v},\ t)$ in the phase space determined by $\mathbf{v}$—that is, we seek the probability that a neuron of the population is in a state $\mathbf{v}$ at a time t. To determine ρ, we imagine a large number of replicas—say, N—of the direct simulation. As discussed in the previous section, the connectivity matrix is drawn from an ensemble, and so also is the external stimulus. Both of these can be thought of as generating N replicas of the population. If $d\mathbf{v}$ is a small volume in the phase space, so that $n_k(\mathbf{v},\ t)\, d\mathbf{v}$ is the number of neurons in $d\mathbf{v}$, at time t of the kth replica, then the number density at $\mathbf{v}$ is defined as

$$n(\mathbf{v}, t) = \langle n_k \rangle = \lim_{N \uparrow \infty} \frac{1}{N} \sum_k n_k(\mathbf{v}, t), \qquad (10)$$

and

$$\rho(\mathbf{v}, t) = \frac{n(\mathbf{v}, t)}{\int n(\mathbf{v},\ t)\, d\mathbf{v}} = \frac{n(\mathbf{v}, t)}{P} \qquad (11)$$

is the required probability density, where P is the number of neurons in each replicate population.

In preparation for the derivation of the equation that governs ρ, we calculate the average firing rate per neuron, $r(t)$. As above, if $\{t_n^m\}$ designates the firing times of the mth neuron the firing rate is given by

$$r(t) = \frac{1}{P} \lim_{\triangle t \downarrow 0} \left\langle \frac{1}{\triangle t} \int_t^{t+\triangle t} dt \sum_{m \neq 0} \sum_n \delta\left(t - t_n^m\right) \right\rangle, \qquad (12)$$

where, as in (10), $\langle\ \rangle$ denotes an average over the ensemble of replicas. In the same way, the part of the arriving firing rate that is due to the external sources will be denoted by a zero superscript and is given by

$$\sigma^0(t) = \lim_{\triangle t \downarrow 0} \left\langle \frac{1}{\triangle t} \int_t^{t+\triangle t} dt \sum_n \delta\left(t - t_n^0\right) \right\rangle. \qquad (13)$$

Thus a neuron feels, on average, the impulse rate

$$\sigma(t) = \sigma^0(t) + Gr(t), \qquad (14)$$

where, as in the previous section, G is the (average) number of afferents. Equation (14) might be referred to descriptively as a *dynamic mean field* approximation

(Gerstner, 1995; see also Schuster and Wagner, 1990, for an earlier mean field approach). Next, denote by D a small enough fixed volume in $\mathbf{v}$ space, and consider the time rate of change of the number of elements in D. This is given by

$$\frac{\partial}{\partial t}\int_D \rho\, d\mathbf{v} = -\int_{\partial D} \mathbf{F}(\mathbf{v})\cdot\mathbf{n}\rho\, d\omega - \int_D d\mathbf{v}\left(\frac{\delta\rho}{\delta t}\right)^-_{imp} + \int_D d\mathbf{v}\left(\frac{\delta\rho}{\delta t}\right)^+_{imp}. \quad (15)$$

The first term on the right is the rate of loss of probability within D ($\mathbf{n}$ is the outward normal to the surface ∂D for which $d\omega$ is a surface element) due to the streaming term of (1), $\mathbf{F}(\mathbf{v})$. The next two terms represent the effect of synaptic impulses—that is, the contribution arising from $\mathbf{S}(\mathbf{v}, g(t))$ in (1); hence the subscript *imp*. The first of these is the loss rate, and if we take D small enough so that any neuron within D leaves D on receiving an impulse, then the loss rate is given by[1]

$$\left(\frac{\delta\rho}{\delta t}\right)^-_{imp} = \sigma(t)\rho(\mathbf{v}, t). \quad (16)$$

At the time of a synaptic impulse the conductivity experiences a delta function. Therefore, the responding membrane potential is discontinuous, but all other elements of $\mathbf{v}$ are continuous. If V is the potential, and after an impulse it becomes V', then we write

$$(V, v_2, v_3, \ldots) = \mathbf{v} \to \mathbf{v}' = (V', v_2, v_3, \ldots). \quad (17)$$

The relation between V and V' follows from integrating the first equation of (1) (the membrane potential equation) across the instant of the impulse. For the particular forms shown in (2) and (9), this yields

$$V' = V + h, \quad (18)$$

where we have assumed that $\hat{g}$ and $h = \hat{g}V_s/C$ are small. Thus the volume D goes to a volume—say, D'—under (18). See Fig. 1 for a schematic illustration.

These observations indicate how to construct the gain rate that is the last term of (15). For this purpose we consider the volume D'', constructed so that if $\mathbf{v}''\epsilon D''$, then under an impulse it goes into D, symbolically

$$\mathbf{v}''(D'') \to \mathbf{v}(D). \quad (19)$$

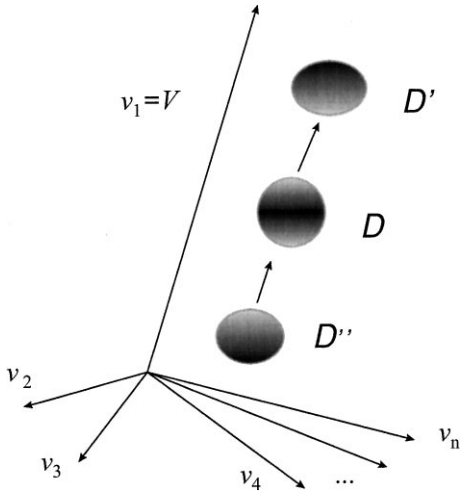

Figure 1. Phase space defined by the state vector $\mathbf{v} = (v_1, \ldots, v_n)$ of an individual neuron. Phase points in region D'' representing neurons are bumped by synaptic impulses into region D. They are similarly removed from D into D'.

See Fig. 1. Since only the membrane potential changes under an impulse, we make the substitutions $V \to V'$, $V'' \to V$ in (18) and solve for V'' to obtain

$$V'' = V''(V) = V - h. \quad (20)$$

It then follows that the gain rate is

$$\int_D \left(\frac{\delta\rho}{\delta t}\right)^+_{imp} d\mathbf{v} = \sigma(t)\int_{D''} \rho(\mathbf{v}'')\, d\mathbf{v}'' = \sigma(t)\int_D \rho(\mathbf{v}''(\mathbf{v}))\frac{\partial\mathbf{v}''}{\partial\mathbf{v}}\, d\mathbf{v}, \quad (21)$$

where to obtain the last expression we have transformed from D'' to D, and thus the Jacobian of the transformation, $\partial\mathbf{v}''/\partial\mathbf{v}$, appears.

To complete the derivation we observe that since D is small but otherwise arbitrary, it follows that

$$\frac{\partial\rho}{\partial t} = -\frac{\partial}{\partial\mathbf{v}}\cdot(F(\mathbf{v})\rho) - \sigma(t) \times\left\{\rho(\mathbf{v}, t) - \rho(\mathbf{v}''(\mathbf{v}), t)\frac{\partial\mathbf{v}''}{\partial\mathbf{v}}\right\}. \quad (22)$$

We observe that for the particular case indicated by (20),

$$\frac{\partial\mathbf{v}''}{\partial\mathbf{v}} = \frac{\partial V''}{\partial V} = 1. \quad (23)$$

If we define

$$\mathbf{J}_{imp} = -\sigma(t) \int_V^{V''(V)} \mathbf{e}_V \rho(W, v_2, \ldots)\, dW, \quad (24)$$

where $\mathbf{e}_V$ is the unit vector in the V-direction and

$$\mathbf{J}_{str} = \rho \mathbf{F}(\mathbf{v}), \quad (25)$$

then (22) can be written as

$$\frac{\partial \rho}{\partial t} = -\frac{\partial}{\partial \mathbf{v}} \cdot \mathbf{J}, \quad (26)$$

where $\mathbf{J}$ is the flux

$$\mathbf{J} = \mathbf{J}_{str} + \mathbf{J}_{imp}. \quad (27)$$

The form (27) is convenient for formal purposes.

Thus we see that the flux $\mathbf{J}$ has the form of a linear operator acting on the density

$$\mathbf{J} = \mathbf{C}(\sigma)\rho, \quad (28)$$

where as indicated the linear operator depends on the incoming firing rate.

The firing of a single neuron can be based on the action potential reaching its maximum. This criterion is inconvenient for dealing with populations. Alternatively the firing rate per neuron of the population, r, can be determined by the flux of neurons of the population passing a threshold. It therefore is a functional of $\mathbf{J}$,

$$r(t) = R[\mathbf{J}]. \quad (29)$$

To determine r construct a Poincaré surface at a threshold value of the potential and determine the flux through this surface. Because r, through (28) and (29), is a functional of ρ and, through (14), contributes to σ which appears in (28), the problem is nonlinear. Nevertheless, the framework for dealing with the population equation is largely determined by linear theory.

Integration of (26) over the domain, Đ of the dynamical space yields

$$\frac{\partial}{\partial t} \int_{Đ} \rho(\mathbf{v})\, d\mathbf{v}' = -\int_{\partial Đ} \mathbf{n} \cdot \mathbf{J}\, dS, \quad (30)$$

where $\partial Đ$ refers to the bounding surface of Đ. Đ contains all possible trajectories of the dynamical system. We require that the probability be conserved so that

$$\int_{\partial Đ} \mathbf{n} \cdot \mathbf{J}\, dS = 0. \quad (31)$$

A resting state surface may be introduced in analogy with the threshold surface, as is the case for the integrate-and-fire example. If this is done, then Đ has a segment removed and condition (31) is met, if the probability flux leaving the *threshold surface* equals the probability flux entering the *reset surface*. As we will see in the next section, for integrate-and-fire dynamics this can require additional boundary conditions.

The above deliberations show that exactly as in statistical mechanics, the population dynamics is derived from the dynamics of individual units with the addition of a reasonable assumption of a statistical nature. No free parameters or constants enter into this relationship.

We will discuss further details of the population equation for specific cases in Section 5 below. For the moment we present the generalization to interacting subpopulations. Suppose each subpopulation is described by its own probability density

$$\rho_k = \rho_k(\mathbf{v}, t), \quad k = 1, 2, \ldots, M, \quad (32)$$

each with a probability flux

$$\mathbf{J}_k = \mathbf{C}_k\big(s_k^0, r_1, \ldots, r_M\big)\rho_k, \quad (33)$$

which satisfies the continuity equation

$$\frac{\partial \rho_k}{\partial t} = -\frac{\partial}{\partial \mathbf{v}} \cdot \mathbf{J}_k, \quad k = 1, 2, \ldots, M. \quad (34)$$

Here $s^0 = s^0(t)$ denotes the external firing rate to the kth population and r_k, the firing rate of the kth population is a functional of $\mathbf{J}_k$,

$$r_k = R[\mathbf{J}_k], \quad k = 1, 2, \ldots, M. \quad (35)$$

This general form allows for each subpopulation to receive excitatory (and inhibitory) input from all subpopulations. In the interest of simplicity, we will not go into details of weighting and connectivity.

It should be observed that the formalism applies independently of the detailed model of the population. This is also taken up in Knight (1998).

5. Integrate-and-Fire Model

We now specialize the above deliberations to the case of integrate-and-fire dynamics, (5). The probability flux is now given by

$$J = -\gamma v\rho(v,t) + \sigma(t)\int_{v-h}^{v}\rho(v')\,dv'. \quad (36)$$

Here h represents a normalized form that occurs in (18). Since each impulse arrival elevates the membrane potential by an increment h, the current that appears in the integrate-and-fire equation, (5) is given by

$$s = \sigma h = (\sigma^0 + Gr)h. \quad (37)$$

The population equation is

$$\frac{\partial\rho}{\partial t} = \gamma\frac{\partial(v\rho)}{\partial v} + \sigma(t)\{\rho(v-h) - \rho(v)\}. \quad (38)$$

To obtain this we have used $v'' = v - h$ with a fixed small value for h. The firing rate of the population is simply given by

$$r(t) = J(v=1) = -\gamma\rho(1,t) + \sigma\int_{1-h}^{1}\rho(v')\,dv'. \quad (39)$$

As stated in the previous section one boundary condition, (31), is

$$J(0) = J(1). \quad (40)$$

The presence of the offset term, $\rho(v-h)$, requires another boundary condition. Examination of (39) shows that $r(t)$ the flux of probability at $v=1$ is due to impulses driving neurons past the threshold. This is made up of an integral term and a term due to leakage. The latter is actually a flux to the left and hence cannot really contribute to the firing rate. Hence this requires

$$\rho(v=1,t) = 0, \quad (41)$$

which is the necessary additional boundary condition.

Next, if (14) is substituted into (39) and (41) imposed, we find

$$r(t) = \frac{\sigma^0(t)\int_{1-h}^{1}\rho(v')\,dv'}{1 - G\int_{1-h}^{1}\rho(v')\,dv'}, \quad (42)$$

and therefore (38) maybe rewritten as

$$\frac{\partial\rho}{\partial t} = \gamma\frac{\partial(v\rho)}{\partial v} + \frac{\sigma^0(t)}{1 - G\int_{1-h}^{1}\rho(v')\,dv'} \times\{\rho(v-h) - \rho(v)\}. \quad (43)$$

This form clearly illustrates that the problem is governed by a nonlinear integral-differential equation. In this respect it is akin to the Boltzmann equation of statistical mechanics.

We conclude this section with three extensions that figure in the examples that are discussed in the next section.

Stochastic Jumps

First we wish to include the effect of stochastic jumps in response to neuronal impulses. If we denote the probability of a voltage jump h by $p(h)$, then evidently (38)

$$\frac{\partial\rho}{\partial t} = \gamma\frac{\partial(v\rho)}{\partial v} - \sigma(t) \times\left\{\rho(v) - \int_0^v dh p(h)\rho(v-h)\right\}. \quad (44)$$

Another form is

$$\frac{\partial\rho}{\partial t} = -\frac{\partial}{\partial v}\left\{-\gamma v\rho + \sigma(t)\int_0^v \tau(v-v')\rho(v')\,dv\right\}, \quad (45)$$

where

$$\tau(h) = \int_h^1 p(h')\,dh'. \quad (46)$$

Inhibition

To illustrate how inhibitory interactions may be introduced by following the general formulation in the previous section, let us assume that (18) has the special form $v' = v(1-\kappa)$, and hence (19) becomes $v'' = v/(1-\kappa)$. This places the reversal potential for synaptic inhibition at the origin $v = 0$, where the leakage and reset equilibrium potentials also are located in our integrate-and-fire model. Further assume that the probability of connection is distributed uniformly over all neurons. For a given neuron, then, the

fraction of postsynaptic neurons that are excitatory is simply equal to the fraction, f, of excitatory neurons in the population. Consequently, the probability flux is expressed as

$$J = -\gamma v\rho + [\sigma^0(t) + Gfr\,(t)] \int_{v-h}^{v} \rho(v')\,dv' - G(1-f)r(t) \int_{v}^{v/(1-\kappa)} \rho(v')\,dv' \qquad (47)$$

instead of (36). The constant κ is small and will be discussed later. For a general treatment, we should consider inhibitory and excitatory neurons as separate populations. Purely for expository reasons we have chosen uniform probability of connections that results in (47). Further generalizations can be included in the framework of the more general format considered in Section 4.

Diffusion Approximation

Finally, the diffusion limit will be considered for purposes of comparison. Simply stated, for $h \downarrow 0$ we can consider the Taylor expansion

$$\int_{v-h}^{v} \rho(v')\,dv' \approx h\rho - \frac{1}{2}h^2\frac{\partial}{\partial v}\rho. \qquad (48)$$

If this expansion is inserted in (36), we obtain instead of (38) the diffusion equation

$$\frac{\partial\rho}{\partial t} = \frac{\partial}{\partial v}(\gamma v - \sigma h)\,\rho + \frac{\sigma}{2}h^2\frac{\partial^2}{\partial v^2}\rho = \frac{\partial}{\partial v}(\gamma v - s) + s\frac{h}{2}\frac{\partial^2}{\partial v^2}\rho. \qquad (49)$$

6. Simulations

The purpose of this section is to compare solutions of the population equation with the results of the direct simulation. Since the population equation is derived essentially from the same assumptions that specify the direct simulation (but see note 1), the results of the two views should converge as the number of neurons P becomes large. To verify this and to explore the population approach, we have numerically solved the partial differential equation that describes the evolution of the probability density. Concurrently, the direct simulation is performed by solving large sets of ordinary differential equations each of which represents an individual neuron. Details of the numerical methods are provided in the appendix.

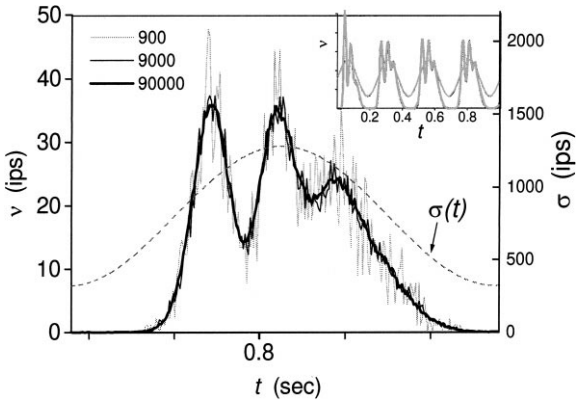

Figure 2. The firing rates ν, of three populations consisting of 900, 9,000, and 90,000 neurons. They are driven by a sinusoidally modulated input with mean frequency σ, shown as the dashed curve. Neuron firings have been averaged over each millisecond. Main figure shows the last of the four periodic oscillations shown in the inset. As the number of neurons is increased, the random fluctuations in the firing rate diminish as the square root of population size. The populations receive no feedback.

To demonstrate the effect that the number of neurons has on the results of the direct simulation, we compare the time-dependent firing rate of three direct simulations containing 900, 9,000, and 90,000 neurons. The results are shown in Fig. 2. Each population in the figure consists of an uncoupled set of leaky integrate-and-fire neurons described by (5). The synaptic input to every neuron is purely external and consists of individual Poisson distributed impulses arriving with a time-dependent mean frequency, σ. For the cases shown the frequency is sinusoidally modulated in accordance with $\sigma(t) = \sigma_0(1 + B\sin(\omega t))$ where $\sigma_0 = 800\ s^{-1}$, $B = 0.6$, and $\omega = 8\pi s^{-1}$. In this calculation the impulse strength is kept at the constant $h = 0.03$. In this and all subsequent calculations we have taken the ohmic time constant to be $\gamma = 20\,s^{-1}$.

To examine fine details in the evolution of the population activity, Fig. 2 focuses on a time interval that spans one full period of the synaptic input. The starting transient has been allowed to die away and leaves only the periodic oscillation. Neuron firings have been averaged over each millisecond. In Fig. 2 the population with 90,000 neurons displays irregular fluctuations that are an order of magnitude smaller than those produced by the population with 900 neurons. Thus the figure supports the expectation that the average magnitude of the irregular fluctuations decreases as

the square root of the number of neurons in the population.

The population of 90,000 neurons in Fig. 2 reveals most clearly the underlying smooth variations in the firing rate. Systematic changes have the same period as the input $\sigma(t)$. In addition, we observe that the firing rate initially increases with the input. Then it reaches its first peak at $t = 0.77$ even though the input continues to rise. This and the following downturn may be explained as follows. The average time it takes a neuron to cross the domain $0 < v < 1$, the transit time, can be estimated as the reciprocal of the firing rate. In the initial period the mean firing rate is about 30 *ips*. The transit time is thus about .033 *s*, which corresponds to the interval between the first two peaks. At the first peak a large fraction of the neurons have fired and have been reintroduced at the origin. Thus the second peak occurs when these reappear at threshold. Similarly, the third peak in part is diminished due to the slower mean firing rate present at the occurrence of the third peak. Finally, the mean rate becomes too small to overcome leakage and the firing rate drops to nearly zero.

We now compare these results with the firing-rate calculations that follow from the population Eq. (38) under the same conditions as those of the simulation. We plot the results of the population equation with the direct simulation. Figure 3 shows that there is

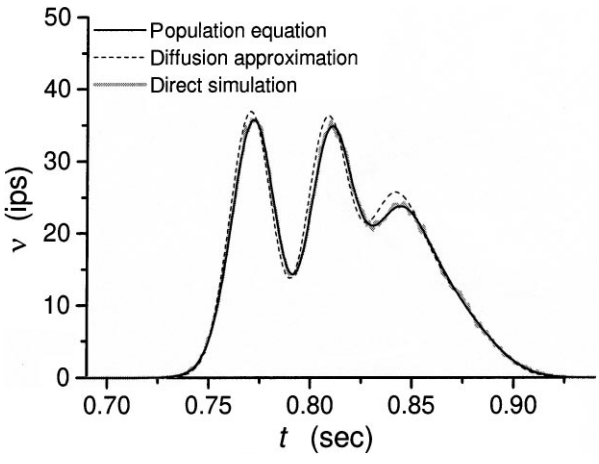

Figure 3. The firing rate ν of the directly simulated population with 90,000 neurons shows small fluctuations about the smooth curve predicted by the population equation. The diffusion equation gives a firing rate with significant deviations. The time period shown and the input are the same as in Fig. 2. The populations contain no feedback.

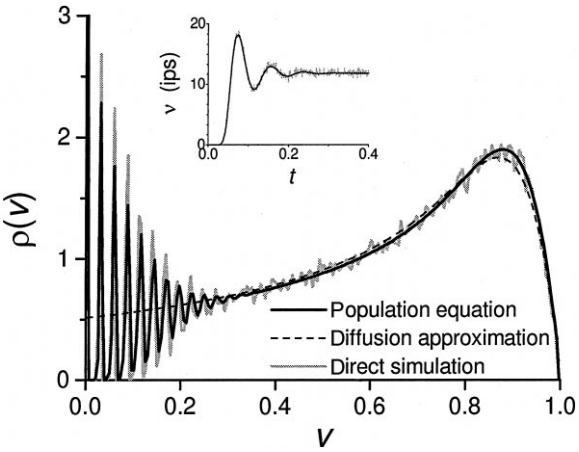

Figure 4. The probability density at equilibrium given by a direct simulation of 90,000 neurons, the population equation, and the diffusion approximation. The state shown in the main figure is reached at the end of the period shown in the inset. The inset shows the firing rates of the direct simulation and population equation as they converge on the steady state. The input is a step current with $\sigma = 800$ ips starting at $t = 0$. The populations contain no feedback.

excellent agreement in the firing rates for the two methods throughout the time-course. The figure shows, in addition, that the firing rate predicted by the diffusion approximation contains significant deviations from the other calculations. As would be predicted, we have found that these deviations in the diffusion approximation decrease as the value of h used in the model becomes smaller.

Next we consider the response to a step increase in the driving term, $\sigma^0(t)$, from 0 to 800 s^{-1} at $t = 0$. Figure 4 presents a comparison between the direct simulation and the corresponding results obtained with the population Eq. (38) for $G = 0$ for the asymptotic time-independent equilibrium state, $\rho_0(v)$. In the case shown, the initial condition was a delta function of unit strength located at the origin. The inset in Fig. 4 shows the transient firing rate of the population as it oscillates about its equilibrium value within an exponentially diminishing envelope. To explain the order of magnitude of the response, it is useful to note that, in the absence of leakage ($\gamma = 0$), the firing rate would equal 24 ips. It follows naturally that the firing rate obtained in the numerical solution is somewhat lower than this value since leakage is included ($\gamma = 20\, s^{-1}$) in our equations. The firing rate of the population at equilibrium without feedback can be evaluated analytically and equals 11.82 s^{-1} in this case (Sirovich et al., 1998). The main part of Fig. 3 shows the probability density at

equilibrium. The figure indicates that the firing rate and the probability density obtained by the population equation are in excellent agreement with the direct simulation.

Figure 4 shows that near the origin the equilibrium probability density contains severe excursions that decrease and finally disappear as v increases. These excursions in $\rho_0(v)$ are due to the behavior of the neurons shortly after reentering the unit interval at the origin after reaching the threshold at the right. Similar structures were discovered by Wilbur and Rinzel (1982). The membrane potential is incremented by a step of size h at every Poisson-distributed impulse, and decays smoothly due to leakage during each stochastically distributed interpulse interval. The accumulation of random amounts of leakage eventually washes out the concentration of neurons at multiples of h. A full mathematical discussion of the equilibrium solution is presented in Sirovich et al. (1998).

Figure 5 shows that the oscillations in $\rho_0(v)$ are much smaller if the steps h are distributed randomly. In Fig. 5 the impulse strengths are distributed normally around the value they have in Fig. 4 with a fixed standard deviation. A probability distribution

$$p(h) \propto \begin{cases} \exp[-(h-\bar{h})^2/(2\alpha^2)] & \text{if } h \geq 0 \\ 0 & \text{if } h < 0 \end{cases} \tag{50}$$

with $\bar{h} = 0.03$ and $\alpha = 0.3\bar{h}$ has been used in (44) to calculate the evolution of the probability density.

The equilibrium probability densities as shown in Figs. 4 and 5 each include a delta function at the origin.

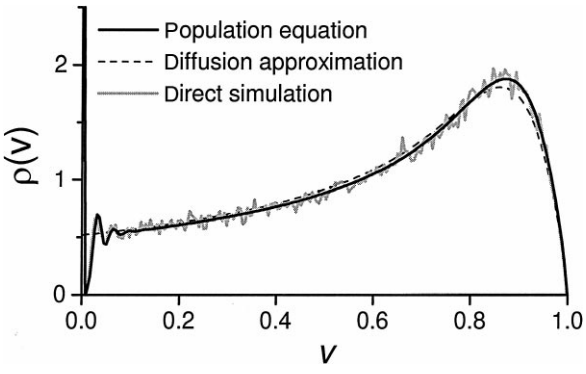

Figure 5. Same as Fig. 4 with the exception that the voltage step h is a random variable Gaussian distributed around the value $\bar{h} = 0.03$ (used in previous figures) and standard deviation equal to 30% of $\bar{h}$. In comparison with the result in Fig. 4, the oscillations in ρ near $v = 0$ are drastically reduced The population has no feedback.

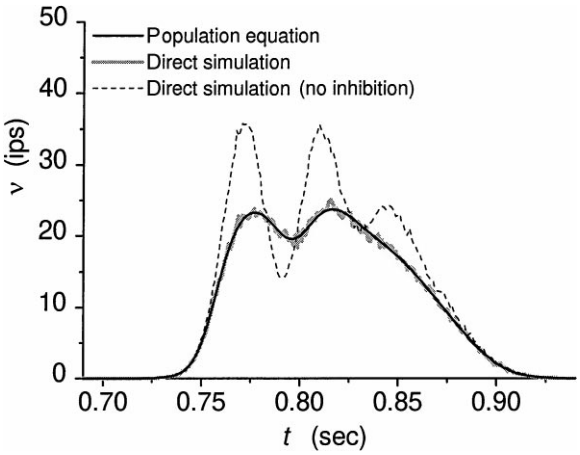

Figure 6. The firing rates of a directly simulated population with 90,000 neurons and the population equation with inhibitory and excitatory feedback are shown. The number of outgoing connection per neuron $G = 10$ and 80% of all neurons are inhibitory. The uncoupled populations firing rate from previous figures is included as the dashed curve for comparison. The input and the time window shown are the same as in Figs. 2 and 3.

This reflects the fact that on the average there is in the population a finite number of neurons located exactly at the origin. Figures 4 and 5 also show the probability density obtained from the population equation at the diffusion limit (49).

The model has also been tested with a fixed fraction of inhibitory neurons present in the population. In Fig. 6 we show, as an example, a numerical experiment performed with the same external stimulus as in Figs. 2 and 3. Every neuron in this population is connected to $G = 10$ postsynaptic neurons in the same population. The fraction of neurons that are excitatory has been set to the value $f = 0.2$ in (47). As Fig. 6 indicates, the presence of inhibitory connections depresses the firing rate in relation to the results obtained from the decoupled population. The direct simulation for the latter is included in the figure for comparison. The figure again shows excellent agreement between the direct simulation and the population equation.

Finally, we mention that the methods presented here have been applied by us to the modeling of an orientation hypercolumn (Omurtag et al., 1999). The model incorporated the *wiring* that appears in the study by Somers et al. (1995). Our results showed remarkable qualitative agreement with the cortical dynamics of V1 as recently found by Ringach et al. (1997). A fuller report on these simulations is in preparation.

Acknowledgment

The authors wish to gratefully acknowledge helpful conversations with E. Kaplan. We also wish to acknowledge the constructive criticism of two excellent referees, one of whom suggested the term *dynamic mean field* used in the text. This work was supported by NIH/NIMH MH50166, NIH/NEI EY11276, ONR N00014-96-1-0492, ONR N0014-96-1-5005.

Appendix

Numerical Methods

Population Equation. In our model the state space of a neuron is simply the rescaled membrane potential v in (5), which ranges over the unit interval. We first define $\Delta v = 1/N$ and $v_i = i\Delta v$. The grid points (or nodes) where the probability density and the flux are represented are staggered with respect to one another: we define $\rho_i(t) = \rho(v_i - \Delta v/2, t)$ and $J_i(t) = J(v_i, t)$. With this notation the continuity Eq. (26) can be written as

$$\frac{\partial \rho_i}{\partial t} = -\frac{J_i - J_{i-1}}{\Delta v} + O[(\Delta v)^2]. \tag{51}$$

Here we focus on the case of stochastic jumps. The expression for flux that appears in (45) is discretized as

$$J_i(t) = -\gamma v_i \frac{\rho_i + \rho_{i+1}}{2} + \sigma(t)\Delta v \sum_{k=1}^{i} \rho_k q_{k-i} + O[(\Delta v)^2], \tag{52}$$

where

$$q_{k-i} = \frac{1}{2}\, erfc\left\{ \frac{[v_k - (v_i - \bar{h})]^2}{\sqrt{2}\alpha} \right\} \tag{53}$$

is the discretization of τ in (46) with $p(h')$ taken as in (50). In this expression, $\bar{h}$ and α are the mean and standard deviation of the strength of delta impulses. The firing rate of the population is obtained from the expression for flux by letting $i = N$.

As a standard numerical technique for implementing the right boundary condition (41) for the probability density, we include an additional node, $N+1$, in the computational domain at $v = 1 + \Delta v/2$, where $\rho_{N+1}(t) = -\rho_N(t)$. This ensures that the probability density vanishes at the right boundary with second-order accuracy. When this is used in the expression for $J_N(t)$, the flux associated with leakage is seen to be zero. For $i = 2, \ldots, N$, (45) is discretized as

$$\frac{\partial \rho_i}{\partial t} = \frac{\gamma}{2}[-(i-1)\rho_{i-1} + \rho_i + i\rho_{i+1}] - \sigma(t)\left[\rho_i q_0 + \sum_{k=1}^{i-1} \rho_k (q_{k-i} - q_{k+1-i})\right] + O[(\Delta v)^2]. \tag{54}$$

This equation does not apply at the first node, $i = 1$. There the periodic boundary condition (40) on flux, $J_0(t) = J_N(t)$, must be used along with the continuity Eq. (51).

Eq. (54) and the equation for $i = 1$ are of the form

$$\frac{\partial \rho_i}{\partial t} = \sum_{j=1}^{N} \left[A_{ij}^{(0)} + \sigma(t) A_{ij}^{(1)}\right]\rho_j, \quad i = 1, \ldots, N. \tag{55}$$

The constant matrices $A_{ij}^{(0)}$ and $A_{ij}^{(1)}$ are associated with leakage and excitatory behavior, respectively. For the sake of brevity inhibitory input to the population described by (47) was not included in this description. Its effect is represented in our computations by an additional matrix multiplying the probability vector in the above equation.

We note here that the probability vector must satisfy $\sum_i \partial \rho_i / \partial t = 0$. This confers on the above matrices the property $\sum_i A_{ij}^{(k)} = 0$, for all j and k. That is, every column of each matrix must sum to zero. This general requirement is satisfied by (54).

The above sets are N-coupled (nonlinear with feedback) ODEs. They are solved by a standard second-order explicit Runge-Kutta scheme. In the computations in this article we have found that $N = 100$ and $\Delta t = 10^{-5}$ result in near convergence of the calculations. Since the computational load is light, we have used $N = 210$ and $\Delta t = 10^{-5}$. In the figures, firing rates are averaged over every 10^3 time steps.

Direct Simulation. In the direct simulations a set of ordinary differential equations (5) are numerically solved simultaneously. In the minimal model the equations are driven by impulses with Poisson-distributed arrival times. The strengths of impulses are distributed according to Eq. (50). In the presence of these sources

of noise a simple and accurate method for numerically performing a direct simulation is to proceed by taking small steps, Δt, in time and to evaluate the membrane potential of each neuron in turn at each time step.

We let Δt be sufficiently small so that the probability of receiving more than one impulse during this time, which is $O[(\Delta t)^2]$, is negligible. For a leaky integrate-and-fire neuron if an impulse with strength h_* arrives at time t_* where $t \leq t_* \leq t + \Delta t$, the membrane potential at the end of the time step is analytically found to be

$$v(t+\Delta t) = v(t)e^{-\gamma \Delta t} + h_* e^{-\gamma (t-t_*)} H(t-t_*), \quad (56)$$

where $H(t - t_*)$ is the Heaviside step function. This we can write as

$$v(t + \Delta t) = v(t)e^{-\gamma \Delta t} + h_* + O[(h_* \gamma \Delta t)]. \quad (57)$$

The algorithm we use for updating the membrane potential of each neuron at every time-step is

$$v(t + \Delta t) = \begin{cases} v(t)e^{-\gamma \Delta t}, & n = 0 \\ v(t)e^{-\gamma \Delta t} + h_*, & n = 1 \end{cases}, \quad (58)$$

where n denotes the number of impulses arriving at a neuron in the interval $(t, t + \Delta t)$. In the present calculations h_* has mean $h = 0.03$, $\gamma = 20\, s^{-1}$, and $\Delta t = 10^{-5}\, s$. Therefore the algorithm has an accuracy of $O[(h\gamma \Delta t)] \sim 10^{-6}$. The firing rate of the population is obtained by simply counting the number of neurons that exceed the threshold during a time-step and dividing this number by the number of neurons in the population. As in the population equation the values of the firing rate given in the figures are averaged over every 10^3 time steps.

Note

1. In expressing this rate as a product in the form (16), we make an assumption of the type called a *Stosszahlansatz* in kinetic theory. In principle, the coefficient of ρ in (16) should be a function of $\mathbf{v}$. This is valid for the gain rate (21) as well.

References

Abeles M (1991) *Corticonics: Neural Circuits of the Cerebral Cortex*. Cambridge University Press, Cambridge.

Abbott LF, van Vreeswijk C (1993) Asynchronous states in networks of pulse-coupled oscillators. *Phys. Rev. E.* 48:1483–1490.

Albrecht TD, Geisler WS (1994) Visual cortex neurons in monkey and cat: Contrast response nonlinearities and stimulus selectivity. *Proceedings SPIE—The International Society for Optical Engineering* 2054:12–31.

Blasdel GG (1992a) Differential imaging of ocular dominance and orientation selectivity in monkey striate cortex. *J. Neurosco.* 12:3115–3138.

Blasdel GG (1992b) Orientation selectivity, preference, and continuity in monkey striate cortex. *J. Neurosci.* 12:3139–3161.

Chawanya T, Aoyagi T, Nishikawa I, Okuda K, Kuramoto Y (1993) A model for feature linking via collective oscillations in the primary visual cortex. *Biological Cybernetics* 68:483–490.

Chee-Orts M-N, Purpura KP, Optican LM (1996) A dynamical model of the primate's early visual pathway: Effect of luminance contrast, spatial scale, and spatial orientation in shaping neuronal firing patterns. Unpublished report.

Everson RM, Prashanth AK, Gabbay M, Knight BW, Sirovich L, Kaplan E (1998) Representation of spatial frequency and orientation in the visual cortex. *Proceedings of the National Academy of Science* 95:8334–8338.

Ferster D, Chuing S, Wheat H (1996) Orientation selectivity of thalamic input to simple cells of cat visual cortex. *Nature* 380:249–252.

Gerstner W. Time structure of the activity in neural network models. *Phys. Rev. E.* 51:738–758.

Gerstner W, van Hemmen JL, Cowan JD (1996) What matters in neuronal locking? *Neural Computation* 8:1653–1676.

Golomb D, Rinzel J (1993) Dynamics of globally coupled inhibitory neurons with heterogeneity. *Physical Review E* 48:4810–4814.

Grinvald A, Bonhoeffer T, Malonek D, Shoham D, Bartfeld E, Arieli A, Hildesheim R, Ratzlaff E (1991) Optical imaging of architecture and function in the living brain. In: Squire LR, Weinberger NM, Lynch G, McGaugh JL., eds. *Memory: Organization Locus of Change.* Oxford: Oxford University Press, Oxford. pp. 49–85.

Hubel DH, Wiesel TN (1962) Reception fields, binocular interaction and functional architecture in the cats visual cortex. *J. Physiol. Lond.* 160:106–154.

Johannesma PIM (1969) *Stochastic Neural Activity: A Theoretical Investigation.* Ph.D. thesis, Nijmegen.

Keener J, Sneyd J (1998) *Mathematical Physiology.* Springer-Verlag, New York.

Knight BW (1972) Dynamics of encoding in a population of neurons. *J. Gen. Physiol.* 59:734–766.

Knight BW (1998) Dynamics of encoding in Neuron populations: Some general mathematical features. Submitted for publication.

Knight BW, Manin D, Sirovich L (1996) Dynamical models of interacting neuron populations. In: Gerf E C, ed. *Symposium on Robotics and Cybernetics: Computational Engineering in Systems Applications*. Cite Scientifique, Lille, France.

Kuramoto Y (1991) Collective synchronization of pulse-coupled oscillators and excitable units. *Physica D* 50:15–30.

McLaughlin D, Shapley R, Shelley M, Wielaard J (1998) Models of neuronal dynamics in the visual cortex. In preparation.

Mirollo E, Strogatz SH (1990) Synchronization of pulse-coupled biological oscillators. *SIAM J. Appl. Math.* 50:1645–1662.

Nykamp D, Tranchina D (1998) A population density approach that facilitates large-scale modeling of neural networks: Analysis

and an application to orientation tuning. Submitted for publication.

Omurtag A, Knight B, Kaplan E, Sirovich L (1999) Efficient simulation of large neuronal populations: An investigation of orientation tuning in the visual cortex. *Invest. Opthalmol. Visual Sci*. 40(4)S3018.

Peskin CS (1975) *Mathematical Aspects of Heart Physiology*. Courant Institute of Mathematical Sciences, New York University, New York.

Ringach D, Hawken M, Shapley R (1997) Dynamics of orientation tuning in macaque primary visual cortex. *Nature* 387:281–284.

Schuster HG, Wagner P (1990) A model for neuronal oscillations in the visual cortex. *J. Biol. Cybernetics.* 64:77–85.

Segev I, Rinzel I, Shepherd G (1995) *The Theoretical Foundation of Dendritic Function: Selected Papers of Wilfrid Rall with Commentaries.* MIT Press, Cambridge, MA.

Singer W, Gray C (1995) Visual feature integration and the temporal correlation hypothesis *Annual Review of Neuroscience.* 18:555–586.

Sillito AM (1975) The contribution of inhibitory mechanisms to the receptive field properties of neurones in the striate cortex of cat. *J. Physiol* 250:305–329.

Sirovich L, Everson R, Kaplan E, Knight, BW, O'Brien E, Orbach D (1996) Modeling the functional organization of the visual cortex. *Physica D* 96:355–366.

Sirovich L, Knight BW, Omurtag A (1998) Dynamics of neuronal populations: The stability of equilibrium solution. Submitted for publication.

Sirovich L, Knight BW, Omurtag A (1999) Dynamics of Neuronal Populations: Stability theory. In preparation.

Somers DC, Nelson SB, Sur M (1995) An emergent model of orientation selectivity in cat visual cortex simple cells. *J. Neurosci*. 15:5448–5465.

Sompolinsky H, Golomb D, Kleinfeld D (1991) Cooperative dynamics in visual processing. *Phys. Rev. A* 43:6990–7011.

Tsodyks M, Mitkov I, Sompolinsky H (1993) Pattern of synchrony in inhomogeneous networks of oscillators with pulse interactions. *Physical Review Letters* 71:1280–1283.

Tuckwell HC (1988) *Introduction to Theoretical Neurobiology*. Cambridge University Press, Cambridge. Vol 2,ch. 9.

Usher M, Schuster HG, Niebur E (1993) Dynamics of populations of integrate-and-fire neurons, partial synchronization and memory. *Neural Computation* 5:570–586.

Wilbur WJ, Rinzel J (1982) An analysis of Stein's model for stochastic neuronal excitation. *Biol. Cybern.* 45:107–114.

Worgotter, F, Koch C (1991) A detailed model of the primary visual pathway in the cat: Comparision of afferent excitatory and intracortical inhibitory connection schemes for orientation selectivity, *J. Neurosci.* 11:1959–1979.